Phase diagrams of a spin-1 Ising system with competing short- and long-range interactions

Octavio D. Rodriguez Salmon
Departamento de Física, Universidade Federal do Amazonas, 3000, Japiim, 69077-000, Manaus-AM, Brazil

J. Ricardo de Sousa
Departamento de Física, Universidade Federal do Amazonas, 3000, Japiim, 69077-000, Manaus-AM, Brazil
and National Institute of Science and Technology for Complex Systems, 3000, Japiim, 69077-000, Manaus-AM, Brazil

Minos A. Neto*
Universidade Federal do Amazonas, Departamento de Física, 3000, Japiim, 69077-000, Manaus-AM, Brazil
(Received 9 April 2015; revised manuscript received 24 August 2015; published 15 September 2015)

We have studied the phase diagrams of the one-dimensional spin-1 Blume-Capel model with anisotropy constant D, in which equivalent-neighbor ferromagnetic interactions of strength $-J$ are superimposed on nearest-neighbor antiferromagnetic interactions of strength K. A rich critical behavior is found due to the competing interactions. At zero temperature two ordered phases exist in the D/J-K/J plane, namely the ferromagnetic (**F**) and the antiferromagnetic one (**AF**). For lower values of $D/J (D/J < 0.25)$ these two ordered phases are separated by the point $K_c = 0.25J$. For $0.25 < D/J \leqslant 0.50$, the paramagnetic phase **P** emerges in a region separated between the lines determined by $D/J = 0.5 - K/J$ and $D/J = K/J$. For $D/J > 0.5$, only phases **AF** and **F** exist and are separated by a line given by $D/J = K/J$. At finite temperatures, we found that the ferromagnetic region of the phase diagram in the k_BT/J-D/J plane is enriched by another ferromagnetic phase $\mathbf{F}'$ above a first-order line for $0.195 < K/J < 0.250$. This first-order line, which separates phases **F** and $\mathbf{F}'$, begins at a coexistence point, where phases **F**, $\mathbf{F}'$, and **P** coexist, and ends at an ordered critical point. Similarly, we found that the phase $\mathbf{F}'$ is present in the phase diagram in the k_BT/J-K/J plane for $0.228 < D/J < 0.286$.

DOI: 10.1103/PhysRevE.92.032120 PACS number(s): 05.70.Fh, 05.70.Jk, 64.60.Kw

I. INTRODUCTION

The systems with competing interactions are very challenging and of great theoretical interest due to their unusual properties [1–5]. For instance, a spin-1/2 Ising model with competing short-range and long-range interactions was used by Kardar [6] to study the crossover from Ising to mean-field criticality, which is a critical phenomenon not only of theoretical interest but also experimental [7]. This particular classical spin system of variables $\sigma_i = \pm 1$ is represented by the following Hamiltonian:

$$\mathcal{H}_{\mathrm{NK}} = -\frac{J}{2N}\sum_{(i,j)}\sigma_i\sigma_j + K\sum_{\langle i,j\rangle}\sigma_i\sigma_j - H\sum_i\sigma_i, \quad (1)$$

where the first sum contains all spin pairs coupled by the positive constant J. The constant J is divided by N to ensure the extensivity [8]. These are called equivalent-neighbor interactions or mean-field interactions. The second sum depends on the dimensionality, because the interactions are only between nearest neighbors. Thus, the parameters K and J denote the short- and long-range interactions, respectively, and H is the external field.

When $K > 0$ and $J > 0$, it emerges a competition between the antiferromagnetic and ferromagnetic couplings. This has been called the Nagle-Kardar (NK) model [9–13]. It is interesting to note that on Bravais lattices any weak equivalent-neighbor interaction changes the nature of the criticality from Ising to mean field [14,15]. However, on the Cayley tree a different phenomenon is found. The infinite-range interaction breaks the universality of the system. Also, in the absence of nearest-neighbor interactions, all spins are equivalent, but the addition of them places the spins in the hierarquical structure of the Cayley tree and it breaks the translational invariance. So the competition between short- and long-range interactions is like a competition between interactions that break the translational invariance and those that preserve it. Kardar and Kaufman found that the reduction of translational invariance (by increasing the strength of the nearest-neighbor couplings) had on the critical behavior the same effect of lowering the spatial dimensionality in Bravais lattices [16].

The one-dimensional case, in zero field, was first solved by Nagle [17], where it was found two ferromagnetic phase transition temperatures. It has been reported, in this case, that the model suffers of ensemble inequivalence and ergodicity breaking [12]. At zero temperature (the ground state), the ferromagnetic phase is present for $K/J < 0.25$ and then the antiferromagnetic phase for $K/J > 0.25$. In the canonical ensemble the model exhibits a tricritical point in the frontier separating the ferromagnetic and paramagnetic phases in the T/J-K/J plane. However, no long-range antiferromagnetic order exists for finite temperatures, though it is present in higher dimensions ($d \geqslant 2$), when K is less than a critical value K_c^{AF}, as shown by Kardar [6].

In order to investigate spin models subject to this type of competition, we investigate in this paper the one-dimensional spin-1 Blume-Capel model [18,19] with competing interactions. This model and its generalization, the Blume-Emery-Griffiths model (BEG), have been proposed to describe the λ transition in ^{4}**He**-^{3}**He** mixtures [20] as well as ordering

*Corresponding author: minos@pq.cnpq.br

in a binary alloy. For dimensions $d \geqslant 2$, the main feature of its phase diagram is the existence of a tricritical point in the plane of temperature versus anisotropy parameter, as has been proved throughout many studies [21–28]. On the other hand, when the spins of the model interact with antiferromagnetic nearest-neighbor couplings, no magnetic order appears at finite temperatures for the one-dimensional case [29], unless an external field is applied to induce the magnetization [30].

The work is organized as follows: In Sec. II we analyze the Blume-Capel model with competing short- and long-range interactions in order to observe how the phase diagram is sensible to the balance of the competing influences. In Sec. III, we discuss the results of the phase diagrams in the k_BT/J-D/J and k_BT/J-K/J planes and the ground-state phase diagrams in the K/J-D/J plane. Section IV is reserved for summarizing and conclusions.

II. MODEL AND METHOD

Recently, Dauxois *et al.* have analyzed models with short- and long-range interactions [31]. In this work was studied the phase diagram of two different Hamiltonians with competing local, nearest-neighbor, and mean-field couplings. We can classify interactions between elementary constituents of matter according to the characteristic potential between two bodies. According to some works in the literature [17,32–34], if this decays at large distance with an exponent that is bigger than the spatial dimension, one speaks of short-range interactions; otherwise interactions are of long range.

Through the years materials that exhibit these characteristics have been studied. For example, Chernyi and coworkers [35] studied the kinetics of a magnetization process in quasi-one-dimensional Ising superantiferromagnet named trimethylammonium cobalt chloride $[(CH_3)_3NH]CoCl_3 \cdot 2H_2O$ (CoTAC) belonging to a wide series of organometallic compounds with general chemical formula $[(CH_3)_3MX_3]CoCl_3 \cdot 2H_2O$ (M = Mn, Co, Ni, Fe, and X = Br, Cl). In the 1970s the effect of a longitudinal field in the Ising antiferromagnet on an anisotropic simple cubic (sc) lattice was studied. The experimental example is the compound $(C_2H_5NH_3)_2CuCl_4$ [36].

One of the attractive points in investigating the properties of $(C_2H_5NH_3)_2CuCl_4$ is that as a consequence of the antiferromagnetic interlayer coupling we may obtain quantitative information about the anisotropy and the exchange coupling J_{AF} by investigating the field dependence of the susceptibility for $T < T_c$. In previous papers [37–40] it has been reported that the Cu compounds of general formula $C_nH_{2n+1}NH_3CuX_4$, where $n = 1$, 2, 3, 4, 5, 6, 10 and X = Cl or Br, can be considered as consisting of nearly isolated magnetic layers.

Compounds of type $(C_nH_{2n+1}NH_3)_2CuCl_4$ have been studied in Refs. [41–43], where the interest was in the observation of intrinsic localized modes. These compounds, organized in a face centered orthorombic crystal, are layered spin strutures, in which the weak magnetic interlayer interaction is antiferromagnetic, between the Cu^{2+} layers, for $n > 1$ and ferromagnetic for $n = 1$. In the ferromagnetic case we have the compound $(CH_3NH_3)_2CuCl_4$, called bis(Methylammonium) tetrachloro-copper [44].

Based on the previous discussions we are interested in improving the study of spin Hamiltonians with competing interactions. Accordingly, we consider a spin-1 chain with long-range and short-range competing interactions, described by the Hamiltonian:

$$\mathcal{H} = -\frac{J}{2N}\left(\sum_{i=1}^{N} S_i\right)^2 + K\sum_{i=1}^{N} S_i S_{i+1} + D\sum_{i=1}^{N} S_i^2, \qquad (2)$$

where $S_i = -1,0,1,\forall i$, and N is the number of spins. As in the NK model, the first term contains the equivalent-neighbor (long-range) interactions and is responsible for the ferromagnetic order if $J > 0$. The second term represents the energy of a linear chain of coupled spins interacting between nearest neighbors. In this paper we choose $K > 0$ to create a competition between short-range and long-range couplings. The third term is the anisotropy term with constant D.

For $K = 0$, we recover the most simple version of the Blume-Capel model [18,19,22]. The results indicate the existence of a phase transition from the high-temperature disordered paramagnetic (**P**) phase to the low-temperature ordered ferromagnetic (**F**) phase at a transition temperature $T_c(D)$ that depends on the values of the anisotropy parameter D. In the limit $D \to -\infty$ one recovers the two-state Ising model with $S_i = \pm 1$. By increasing D, we have a decrease of $T_c(D)$. At zero temperatures, there is a first-transition point $\delta_c = D_c/J = 1/2$, such that for $\delta > \delta_c$ the system exhibits no magnetic order. For $\delta < \delta_c$, one has a first-order transition line, where two different phases coexist (**F** and **P** phases). This coexisting line meets the continuous transition line at a tricritical point (TCP). The **TCP** found for the model (2) for $K = 0$ is located at $\delta_t = \log(4)/3$ and $k_BT/J = 1/3$. In the absence of long-range interactions ($J = 0$), model (2) can be solved by using the matrix transfer technique (see Appendix A), where the system presents no long-range order, i.e., at finite temperatures ($T > 0$) the magnetization is null ($m = 0$). Therefore, the competition between the J (long-range) and K (short-range) interaction tends to cause the appearance of new critical points in the phase diagrams.

In order to study the present model at finite temperatures ($T > 0$), we begin by determining the expression of the partition function Z in the canonical ensemble [45], defined by:

$$Z = \sum_{\{S_i\}} e^{\frac{\beta J}{2N}(\sum_{i=1}^{N} S_i)^2} \prod_{i=1}^{N} e^{-\beta K S_i S_{i+1} - \frac{\beta D}{2}(S_i^2 + S_{i+1}^2)}, \qquad (3)$$

where $\beta = \frac{1}{k_BT}$, k_B is the Boltzmann constant, T is the absolute temperature of the system, and $\sum_{\{S_i\}} \equiv \sum_{S_1=-1}^{1}\sum_{S_2=-1}^{1}\cdots\sum_{S_N=-1}^{1}$ indicates a sum over all spin configurations. Using the Hubbbard-Stratonovich transformation [46,47] in order to reformulate the system of interacting spins into a system in which they are decoupled, obtaining:

$$Z = \sqrt{\frac{N\beta J}{2\pi}} \int_{-\infty}^{\infty} \left\{ e^{-\frac{1}{2}\beta N J x^2} \sum_{\{S_i\}} \prod_{i=1}^{N} e^{\beta \tilde{H}_i} \right\} dx, \qquad (4)$$

where $\tilde{H}_i = \frac{1}{2}Jx(S_i + S_{i+1}) - K S_i S_{i+1} - \frac{1}{2}D(S_i^2 + S_{i+1}^2)$. So the partition function can be calculated by using the

transfer matrix technique that is given by:

$$Z = \sqrt{\frac{N\beta J}{2\pi}} \int_{-\infty}^{\infty} \{e^{-\frac{1}{2}\beta N J x^2} \mathrm{Tr}\{\mathbf{W}^N\}\} dx. \quad (5)$$

This method was used to study the plateau magnetization behavior [30] and to obtain the exact solution of the polymerization problem on the equivalent-neighbor lattice [48]. In the thermodynamic limit ($N \to \infty$) the free energy per spin (free-energy density) is given by (for more details see the Appendix):

$$f(m) = \frac{1}{2} J m^2 - \frac{1}{\beta} \log[\lambda_{\max}(m)] \quad (6)$$

where $\lambda_{\max}(m)$ is the maximum eigenvalue expressed in the Appendix. It is important to emphasize that at the equilibrium, the magnetization m minimizes the free-energy density in Eq. (6) for given values of T, D, and K. So the magnetization can be obtained by equating the partial derivative of the free energy to zero, so:

$$m = \psi(m), \quad (7)$$

where $\psi(m)$ is an expression to be discussed in the Appendix. Furthermore, due to the fact that the Hamiltonian is symmetric under spin reversal in the absence of external field, the free-energy density f can be expanded in even powers of the magnetization. Thus, close to an order-disorder continuous phase transition the Landau expansion of f [45] is given by:

$$f(m) \simeq f_0 + Am^2 + Bm^4 + Cm^6 + O(M^8), \quad (8)$$

where $f_0 = f(0)$, and the coefficients $A, B, C, \ldots$ depend on T, K, and D. The second-order frontiers are obtained by imposing $A(T,K,D) = 0$, with the conditions $B(T,K,D) > 0$ and $C(T,K,D) > 0$. The tricritical point is found when $A(T,K,D) = B(T,K,D) = 0$, with the condition $C(T,K,D) > 0$.

On the other hand, the first-order frontiers can be obtained by Maxwell constructions. In order to avoid metastable states, all solutions obtained were checked to confirm the free-energy minimization. In the following sections we present numerical results for the order parameters and phase diagrams of the model, at both zero and finite temperatures.

The points that appear in our analysis [49] are the following: (i) tricritical points, which signal the encounter of a continuous frontier with a first-order transition; (ii) an ordered critical point, which corresponds to an isolated critical point terminating a first-order line that separates two distinct ordered phases; and (iii) a triple point, signaling the encounter of three first-order critical frontiers. In the phase diagrams we use distinct symbols for the critical points and frontiers, described as follows: continuous (second-order) critical frontier (continuous line), first-order frontier (dotted line), tricritical point: (black circle), ordered critical point (black asterisk), triple point (empty triangle), and five-phase coexistence point (empty diamond).

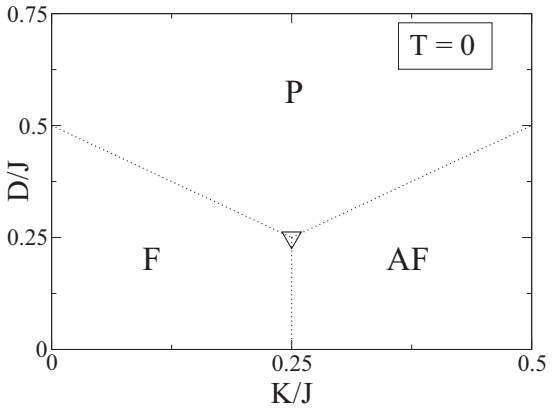

FIG. 1. Ground-state phase diagram in the D/J-K/J plane. The three first-order lines meet at a triple point represented by the empty triangle.

III. RESULTS

A. Ground state

Due to the fact that the second term of free energy $E - TS$ vanishes when $T = 0$, we have to determine the spin configurations which minimize the energy E of the Hamiltonian given in Eq. (2), in order to obtain the frontiers in the D/J-K/J plane. So we proceed as follows: The ferromagnetic phase **F** occurs when all spins point upward ($S_i = 1, \forall i$) or downward ($S_i = -1, \forall i$), and then it has the energy per spin $\epsilon_{\mathbf{F}} = E_{\mathbf{F}}/N = -J/2 + K + D$. For the antiferromagnetic state **AF** consisting of alternate signs of nearest-neighbor spins, the first term of the Hamiltonian gives a vanishing contribution to the energy, so the energy per spin of this phase is $\epsilon_{\mathbf{AF}} = -K + D$. Hence, by imposing $\epsilon_{\mathbf{F}} = \epsilon_{\mathbf{AF}}$ we obtain the transition point $K/J = 1/4$, which separates the **F** and **AF** phases. So we may note that the anisotropy constant D has no influence in the criticality while $0 < D/J < 1/4$. On the other hand, for higher values of $D(D/J > 1/4)$ the magnetic orderings must disappear, so all spins take the value

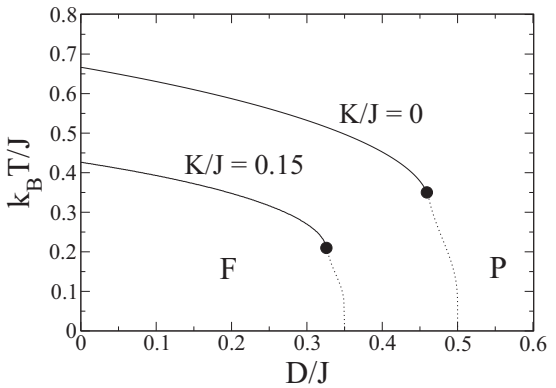

FIG. 2. The phase diagram in the $k_B T/J$-D/J plane corresponding to two values of K/J. For $K = 0$, we can observe the well-known frontier of the Blume-Capel model with ferromagnetic equivalent-neighbor interactions. For $K/J = 0.15$, we may note that the nature of the frontier is still preserved though the ferromagnetic region is reduced.

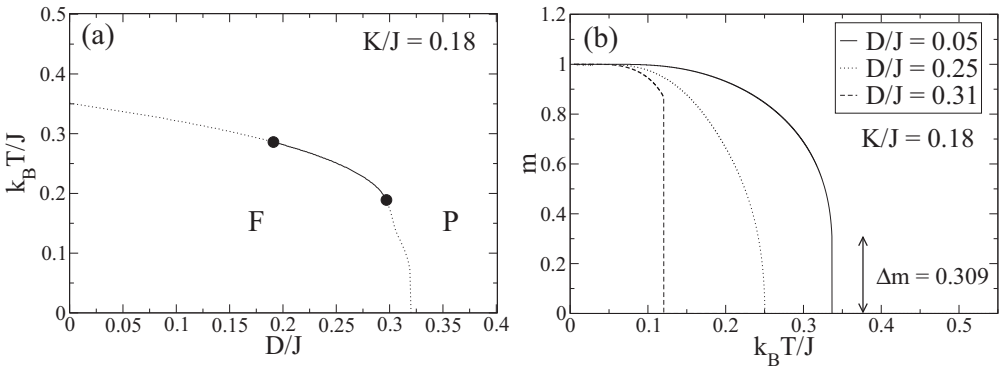

FIG. 3. (a) Phase diagram in the plane of dimensionless variables kT/J versus D/J for $K/J = 0.18$, in which the frontier separating phases **F** and **P** is composed by three lines, two of first-order and one of second-order limited by two tricritical points; (b) the magnetization curve, plotted for three representative values of D/J, for which the magnetization curve crosses three different points of the frontier shown in (a). We observe that for $D/J = 0.05$ and $D/J = 0.31$, the magnetization curves fall discontinuously from $m \neq 0$ to zero, whereas, for $D/J = 0.25$, the magnetization falls continuously to zero.

$S_i = 0$ to minimize the energy E. Thus the system will be in the disordered phase **P**, with energy per spin $\epsilon_{\mathbf{P}} = 0$. Accordingly, by imposing $\epsilon_{\mathbf{F}} = \epsilon_{\mathbf{P}}$ and $\epsilon_{\mathbf{AF}} = \epsilon_{\mathbf{P}}$, we obtain the frontiers **F**-**P** and **AF**-**P**, determined by the first-order lines $D/J = 1/2 - K/J$ and $D/J = K/J$, respectively. In Fig. 1 we show these results in the phase diagram in the D/J-K/J plane for the interval $0 \leqslant K/J < 1/2$.

B. Phase diagram at finite temperatures

At finite temperatures the short-range couplings K of the spin chain cannot establish a spontaneous antiferromagnetic order. However, a ferromagnetic order ($m \neq 0$) can be established below to a critical temperature, due to the presence of the equivalent-neighbor interactions $-J$. Nevertheless, the ferromagnetic order is limited by the values of the parameters K and D, as shown in Fig. 1. So we begin this section by analyzing how the antiferromagnetic couplings K affect the critical behavior of the Blume-Capel model with ferromagnetic equivalent-neighbor interactions.

To this end, we investigate the phase diagrams of the present model in the k_BT/J-D/J plane by scanning them for different values of K/J. So for a given value of K/J, we obtained the phase diagram in the k_BT/J-D/J plane as follows: We first sought the points belonging to a first- or a second-order frontier separating phases with $m \neq 0$ and $m = 0$ by means of a computational algorithm which detects the points $(D/J,k_BT/J)$ where the magnetization given in Eq. (7) changes from $m \neq 0$ and $m = 0$. If the frontier is of first order, then there is a discontinuous change of m, while if the frontier is of second order, the magnetization changes continuously. The accuracy in this detection is $\pm\Delta m$, where $|\Delta m| = 0.001$. Of course, whether a point $(D/J,k_BT/J)$ belongs to a first- or second-order line, one must confirm it by observing the behavior of the free-energy density f versus the magnetization m [see Eq. (6)] at that point or for points around it. For instance, if, for a given value of K/J, a frontier point $(D/J,k_BT/J)$ belongs to a first-order frontier, then the curve of f/J versus m plotted for those values of K/J, D/J, and k_BT/J will show at least two different values of $|m|$, m_1 and m_2, that minimizes f/J, such that $f(m_1) = f(m_2)$. It means that the point $(D/J,k_BT/J)$ in the k_BT/J-D/J plane belongs to a frontier at which two phases coexist. Of course, the first-order frontiers can be obtained numerically by solving simultaneous nonlinear equations [see Eqs. (6) and (7)]. Thus, in order to determine the points $(D/J,k_BT/J)$ of a first-order line

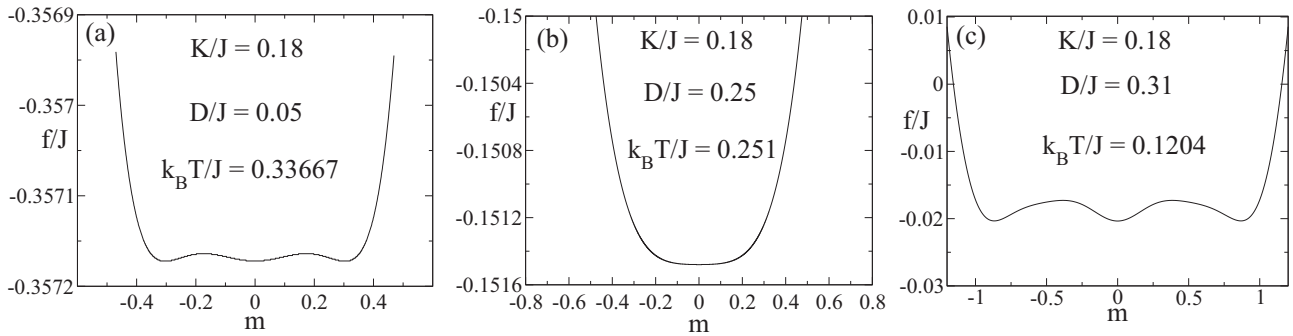

FIG. 4. The free-energy density f plotted as a function of the magnetization, for $K/J = 0.18$, in units of J. In (a), (b), and (c) the minima of f correspond to the critical points where the magnetization curves fall to zero in Fig. 3(b). In (a) the minima coexist for the critical temperature at which the magnetization curve, plotted for $D/J = 0.05$, suffers a discontinuous fall. In (b) f presents one minimum for $m = 0$, for the critical temperature at which the magnetization curve, plotted for $D/J = 0.25$ in Fig. 3(b), falls continuously to zero. In (c) the minima coexist for the critical temperature at which the magnetization curve, plotted for $D/J = 0.31$, suffers a discontinuous fall.

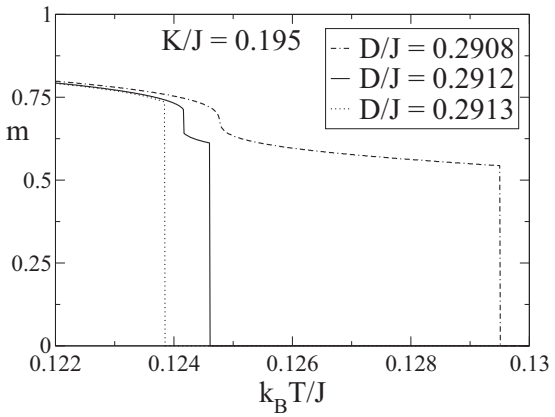

FIG. 5. Three magnetization curves plotted for three different values of D/J for $K/J = 0.195$. The curves plotted for $D/J = 0.2908$ and $D/J = 0.2913$ suffer one discontinuous fall from $m \neq 0$ to $m = 0$. However, for an intermediate value, such as $D/J = 0.2912J$, the magnetization suffers two discontinuous falls. The first one is from $m = m_1$ to $m = m_2$, and the second one is from $m \neq 0$ to $m = 0$. Therefore, a second ferromagnetic phase $\mathbf{F}'$ is present in a small region of D/J for temperatures close to a $\mathbf{F}'$-$\mathbf{P}$ frontier of first order.

separating phases with $m \neq 0$ and $m = 0$, for a given value of K/J, we have to solve the following simultaneous equations:

$$f(m) = f(0) \tag{9}$$

and

$$m = \psi(m), \tag{10}$$

where $\psi(m)$ is discussed in the Appendix. Similarly, to obtain first-order frontiers where two ferromagnetic phases

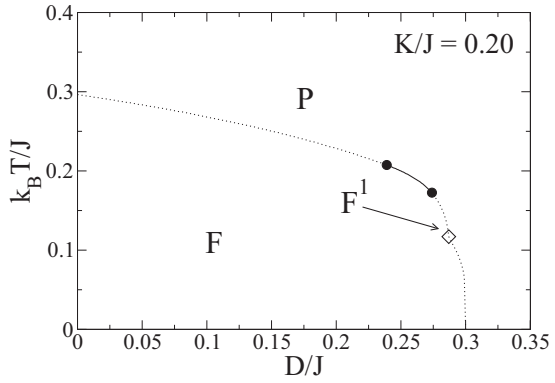

FIG. 6. Phase diagram for $K/J = 0.20$. The intermediate second-order line limited by two tricritical points has been reduced [compare it with that of Fig. 3(a)]. The point, represented by the empty diamond, is a point where two ferromagnetic phases $\mathbf{F}$ and $\mathbf{F}'$ coexist with the phase $\mathbf{P}$. This point gives rise to a coexistent line where phases $\mathbf{F}$ and $\mathbf{F}'$ coexist. This frontier line finishes at an ordered critical point. However, for this value of K/J, the length of this coexistent line is still too short to be observed for this scale of D/J, but it grows as K/J increases. This can be seen in Fig. 7 for a greater value of K/J.

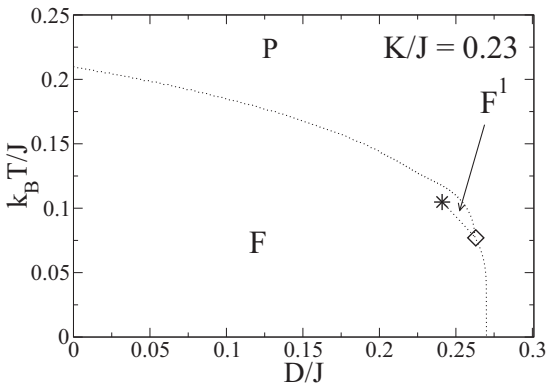

FIG. 7. Phase diagram for $K/J = 0.23$. There is no second-order criticality, as expected for $K/J > 0.204$. A rich critical behavior is shown due to the presence of two ferromagnetic phases $\mathbf{F}$ and $\mathbf{F}'$ separated by a first-order frontier. This frontier begins at a coexistent point represented by an empty diamond, where phases $\mathbf{F}$, $\mathbf{F}'$, and $\mathbf{P}$ coexist, and it finishes at an ordered critical point represented by an asterisk.

$m = m_1$ and $m = m_2$ coexist, their points $(D/J; k_BT/J)$ can be obtained numerically by solving simultaneously

$$f(m_1) = f(m_2), \tag{11a}$$

$$m_1 = \psi(m_1), \tag{11b}$$

and

$$m_2 = \psi(m_2). \tag{12}$$

The second-order frontiers were also obtained by following the Landau's criteria exposed in the preceding section. It is important to avoid spurious solutions, so we plotted the function f/J versus m [see Eq. (6)] to check if the free-energy density was minimized.

Now we will show the results at finite temperatures. In Fig. 2 we show two frontiers separating the ferromagnetic and the paramagnetic phases obtained for two different values of K/J. We may observe that though the ferromagnetic region is reduced by increasing K, the typical topology of the phase diagram of the Blume-Capel model [18,50] is preserved for lower values of K.

However, for $K/J > 0.17$ we observe that the second-order frontier is being reduced when K increases, and it is replaced by a first-order one, as shown in Fig. 3(a). In this figure is shown the phase diagram for $K/J = 0.18$. The frontier that separates the $\mathbf{F}$ and $\mathbf{P}$ phases is now a line containing two tricritical points limiting the second-order line. The new tricritical point came from the left as K/J increases from $K/J = 0.17$, so it appears at the vertical axis $(D/J = 0)$ for $K/J \simeq 0.17$. Then, for $K/J = 0.17$, the second-order line begins to be reduced in the k_BT/J-D/J plane. In the Fig. 3(b) we show the magnetization curves for $K/J = 0.18$, plotted for three representative values of D.

These curves were obtained numerically by solving Eq. (7), and are intended to show how the magnetization curve as a function of the temperature behaves when crossing the three different transitions in the phase diagram shown in Fig. 3(a). Thus, for $D/J = 0.05$, $D/J = 0.25$, and

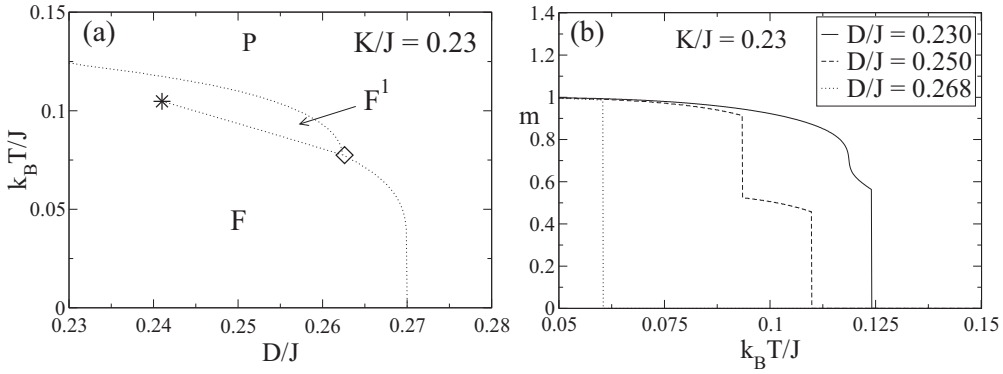

FIG. 8. (a) Phase diagram in the plane of dimensionless variables kT/J versus D/J for $K/J = 0.18$, in which the frontier separating phases **F** and **P** is composed by three lines, two of first-order and one of second-order limited by two tricritical points; (b) the magnetization curve, plotted for three representative values of D/J, for which the magnetization curve crosses three different points of the frontier shown in (a). We observe that for $D/J = 0.05$ and $D/J = 0.31$, the magnetization curves fall discontinuously from $m \neq 0$ to zero, whereas, for $D/J = 0.25$, the magnetization falls continuously to zero.

$D/J = 0.31$ the magnetization curve falls down to zero at $k_BT/J = 0.33667 \pm 0.00001$, $k_BT/J = 0.2510 \pm 0.0002$, and $k_BT/J = 0.1204 \pm 0.0001$, respectively. The accuracies of these temperatures were obtained by scanning the free-energy density (see Fig. 4). Accordingly, for $D/J = 0.05$, the magnetization curve crosses the first-order frontier on the left [see Fig. 3(a)] at the critical temperature $k_BT/J \approx 0.33667$, as shown by the jump discontinuity between the nonzero and zero magnetization ($\Delta m = 0.309$). For $D/J = 0.25$, the magnetization curve crosses continuously the intermediate second-order transition in Fig. 3(a) at the critical temperature $k_BT/J \approx 0.251$, and for $D/J = 0.31$, the magnetization curve crosses discontinously the first-order frontier on the right at $k_BT/J \approx 0.1204$.

In order to confirm the information given in Fig. 3(a), we present the free-energy density versus the magnetization in Fig. 4 plotted for $K/J = 0.18$, corresponding to the frontier points (D/J,k_BT/J) intercepted by the magnetization curves shown in Fig. 3(a). So in Fig. 4(a) we observe that two symmetrical values of the magnetization $\pm m$ minimize the free energy at the same level as $m = 0$ does. This is a signal of a first-order phase transition, in which phases **F** and **P** coexist for the definite values $K/J = 0.18$, $D/J = 0.05$, and $k_BT/J \approx 0.33667$ [see the magnetization curve in Fig. 3(b) plotted for $D/J = 0.05$]. Furthermore, we may observe that phases **F** and **P** are separated by a very small energy barrier ($\Delta f \sim 10^{-5}$). This characterizes the critical points of the first-order line on the left shown in Fig. 3(a). On the contrary, the free-energy density in Fig. 4(c), which belongs to a point of the first-order line on the right, shows that the coexistent phases **F** and **P** are separated by a greater free-energy wall ($\Delta f \sim 10^{-3}$). On the other hand, in Fig. 4(b) we plotted the free-energy density for $D/J = 0.25$ and $k_BT/J \approx 0.251$, which gives us information of the nature of frontier point where the magnetization curve in Fig. 3(b) crosses the second-order frontier for $D/J = 0.25$. Of course, this confirms the second-order criticality of the points of the intermediate line limited by the two tricritical points in Fig. 3(a).

Nevertheless, we observed that this intermediate second-order line disappears in the k_BT/J-D/J plane for $K/J \approx 0.204$. Accordingly, the ferromagnetic zone is limited only by a first-order frontier when $K/J > 0.204$. On the other hand, before the disappearing of this second-order line a second ferromagnetic phase $\mathbf{F}'$ emerges in a small region of the ferromagnetic zone of the phase diagram. This happens because a first-order line separating phases **F** and $\mathbf{F}'$ emerges

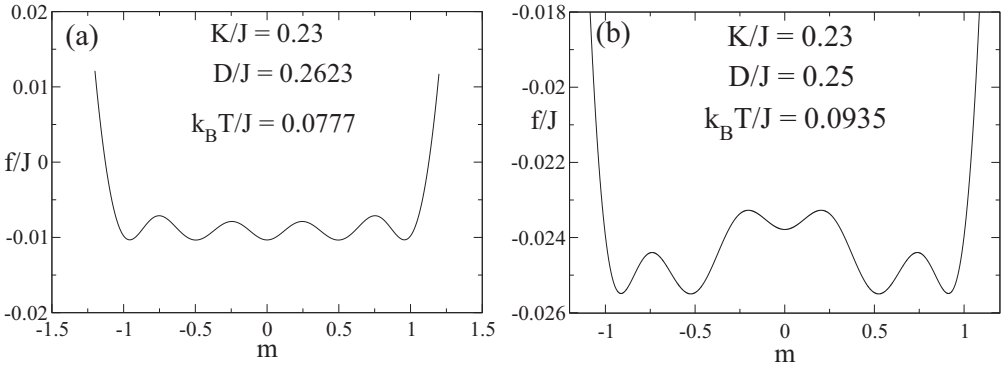

FIG. 9. The free-energy density plotted as a function of the magnetization for $K/J = 0.23$. In (a), the mimima of f/J are at the coexistent point represented by the empty diamond shown in Figs. 7 and 8(a). In (b), the minima are at a point belonging to the **F**-$\mathbf{F}'$ frontier that appeared in Figs. 7 and 8(a).

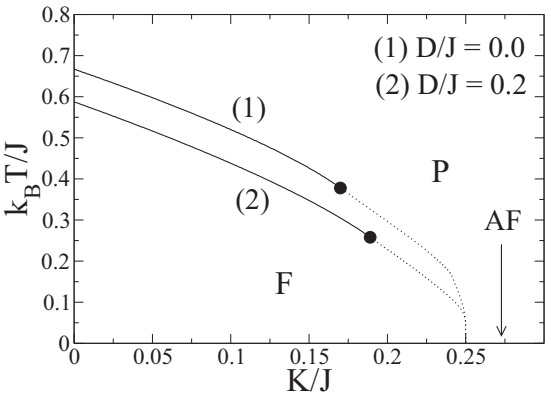

FIG. 10. Frontiers separating the ferromagnetic and the nonferromagnetic region, plotted for $D/J = 0.0$ and $D/J = 0.2$. At zero temperature, the critical value $K/J = 0.25$ divides phases **F** and **AF**.

from a coexistent point where phases **F**, **F**′, and **P** coexist. This begins to happen for $K/J \geqslant 0.195$. In Fig. 5 the magnetization curves plotted for three different values of D/J show that, for $K/J = 0.195$, a second ferromagnetic phase **F**′ appears in a very small interval, $0.2908 < D/J < 0.2913 (\Delta D = 0.0005J)$. This is for temperatures which are between the first-order frontiers $\mathbf{F} - \mathbf{F}'$ and $\mathbf{F}' - \mathbf{P}$.

In Fig. 6, we show the phase diagram for $K/J = 0.20$, where we may observe that the length of the intermediate second-order line has been reduced, so the two tricritical points are closer. Also, we may see the coexistent point represented by the empty diamond, which gives rise to the **F**-**F**′ line. For greater values of K/J, the ferromagnetic region of phase **F**′ is increased. For the sake of visualization, we show in Fig. 7 the phase diagram for $K/J = 0.23$, where we clearly see a first-order frontier separating two ferromagnetic phases. Now we can observe that this frontier begins at the coexistent point represented by the empty diamond and ends at a ordered critical point represented by the asterisk. We can also note that in this phase diagram the second-order frontier is absent because it disappeared for $K/J \approx 0.204$, when the two first-order lines met themselves.

We now concentrate our analysis on describing the most complex region of the phase diagram shown in Fig. 8. Thus, in Fig. 8(a) we show the phase diagram for $K/J = 0.23$, in the interval $0.23 < D/J < 0.28$, to better visualize the most interesting region. So in Fig. 8(b) three different magnetization curves were plotted to confirm the critical behavior in the interval shown in Fig. 8(b). For $D/J = 0.23$ and $D/J = 0.268$, the magnetization curves cross the **F**-**P** frontier. We note that each one presents only one discontinuous fall. However, for $D/J = 0.25$, the magnetization curve presents two discontinuous falls because it crosses the **F**-**F**′ and **F**′-**P** frontiers.

For completeness, we show in Fig. 9(a) the minima of the free-energy density at the coexistent point at which the first-order **F**-**F**′ line begins [see the empty diamond in Figs. 7 and 8(a)]. We can observe there the simultaneous coexistence of phases **F**, **F**′, and P. In Fig. 9(b), the minima of the free-energy density are at a point of the **F**-**F**′ frontier where phases **F** and **F**′ coexist. Finally, for $D/J > 0.5$, no magnetic order exists at finite temperatures.

Before finishing this section we analyze how the anisotropy constant affects the phase transition frontiers separating the region where $m \neq 0$ and $m = 0$. To this end we obtained the phase diagram of the present model in the k_BT/J-K/J plane for different values of the anisotropy parameter D by following the same methodology above. Accordingly, we found essentially three different topologies. The first topology is shown in Fig. 10 where we plotted two frontiers separating the ferromagnetic and the nonferromagnetic region for $D/J = 0$ and $D/J = 0.2$. In this topology a critical point is present. The critical temperature for $K = 0$ decreases as D/J increases. The first-order lines ends at $K/J = 0.25$ at zero temperature.

The second topology begins to appear for $D/J = 0.229$, where the second ferromagnetic phase **F**′ is now present due to the appearance of a second first-order critical line separating phases **F** and **F**′. This line, of course, is similar to that seen in the k_BT/J-D/J plane, beginning at a multicritical point and ending at an ordered critical point. Thus, we show in Fig. 11 the phase diagram for two different values of D/J, in which the phase **F**′ is present. In Fig. 11(a) we show the most complex case of this second topology, obtained for $D/J = 0.25$, in which the first-order line ends at the triple point (at $T = 0$) represented by the empty triangle shown in Fig. 1. In Fig. 11(b) the essential form of the phase diagram is still preserved; however, the antiferromagnetic phase **AF** is no longer present at $T = 0$. Indeed, the phase **AF** does not appear in the plane

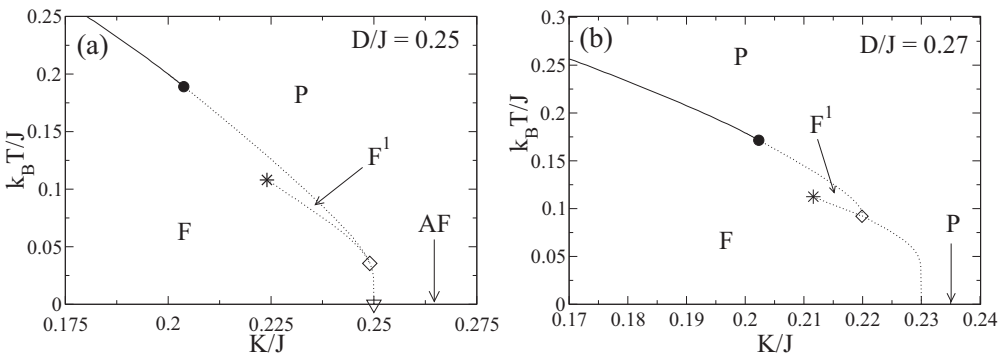

FIG. 11. (a) A portion of the most complex phase diagrams in the plane of dimensionless variables kT/J versus K/J for $D/J = 0.25$; (b) the relevant portion of the phase diagram for $D/J = 0.27$.

k_BT/J-K/J, when $D/J > 0.25$, and is replaced by phase **P**. Thus, the first-order line separating phases **F** and **P** ends now at $K/J = 0.5 - D/J$, for $0.25 < D/J < 0.5$, which is in agreement with the phase diagram depicted in Fig. 1.

For $D/J = 0.286$, the second first-order frontier causing the appearance of phase $\mathbf{F}'$ is no longer present, so the ferromagnetic region is again filled only by phase **F**. So the validity of the second topology is for $0.228 < D/J < 0.286$. Thus, for $D/J > 0.286$, the phase diagram recovers the essential form of the first topology, where there is one tricritical point dividing the second- and the first-order critical lines, and phases **F** and **P** are the only ones which are present. Nevertheless, the second-order frontier disappears for $D/J = 0.462$, as shown in Fig. 11, where we plotted three different frontiers separating phases **F** and **P**, corresponding to three different values of D/J. There we may observe that the trictritical point, represented by the letter **Q**, is at the vertical axis for $D/J = 0.462$. Therefore, the phase diagram has only a first-order line for $0.462 < D/J < 0.5$, as shown by the frontier plotted for the representative value $D/J = 0.49$. This is the third topology found. Of course, no magnetic order is present for $D/J \geqslant 0.5$ (see also Fig. 1). For $D < 0$, the phase diagram is qualitatively similar to the NK model, with the presence of a tricritical point depending on the value of D, where in the limit $D \to -\infty$ we found the same results of Refs. [9–12].

IV. CONCLUSIONS

In summary, we have investigated the critical behavior of the one-dimensional Blume-Capel model with equivalent-neighbor interactions $-J/N$ and nearest-neighbor interactions K. At zero temperature, the phase diagram in the D/J-K/J plane exhibits two ordered phases, the ferromagnetic **F** and the antiferromagnetic **AF** phases, separated by a vertical frontier given by $K/J = 0.25$, for $0 \leqslant D/J \leqslant 0.25$. The paramagnetic phase, denoted by **P**, is present when $D/J > 0.5 - K/J$, for $0 \leqslant K/J \leqslant 0.25$, and when $D/J > K/J$, for $K/J > 0.25$ (see Fig. 1).

At finite temperatures ($T > 0$), no spontaneous antiferromagnetic order is present as expected for a one-dimensional chain of spins. Nevertheless, due to the presence of the equivalent-neighbor ferromagnetic couplings, there exists spontaneous ferromagnetic order for finite temperatures. However, in the k_BT/J-D/J plane, its existence is limited by the values of K/J in the interval $0 \leqslant K/J < 0.25$. For $0 \leqslant K/J \leqslant 0.17$, the qualitative aspect of the Blume-Capel model remains the same (see Fig. 2). In this case $0.17 < K/J \leqslant 0.205$, a second tricritical point appears in the frontier dividing the ferromagnetic and the paramagnetic region [see Fig. 3(a)]. These tricritical points approach themselves as K/J increases. Thus, the second-order line disappears, for $K/J \approx 0.205$, when the two tricritical points meet at the same position.

Accordingly, the whole ferromagnetic-paramagnetic frontier is of first order when $0.205 < K/J \leqslant 0.25$. Also, it was noted that the ferromagnetic region is enriched by the presence of a second ferromagnetic phase $\mathbf{F}'$ for $0.195 < K/J < 0.250$. Nevertheless, the phase $\mathbf{F}'$ is located in a small region limited by a first-order line separating the phases **F** and $\mathbf{F}'$ and the first-order line separating phases $\mathbf{F}'$ and **P** [see Fig. (7)]. So the frontier **F**-$\mathbf{F}'$ begins at a multicritical point where phases **F**, $\mathbf{F}'$, and **P** coexist, and it ends at an ordered critical point, finishing the coexistence of phases **F** and $\mathbf{F}'$. On the other hand, we analyzed the influence of the anisotropy parameter in the phase diagram in the k_BT/J-K/J plane.

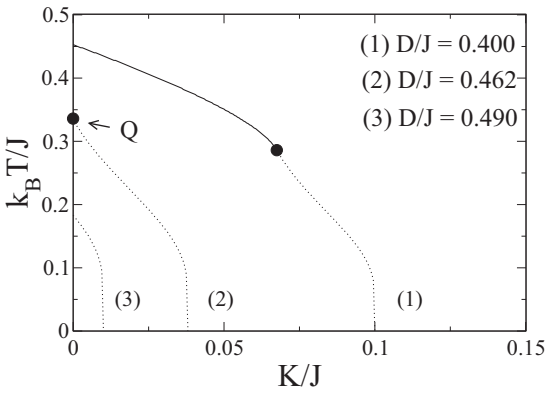

FIG. 12. Frontiers in the plane k_BT/J-K/J separating phases **F** and **P**, plotted for three different values of D/J. The ferromagnetic region is reduced as D increases. So no ferromagnetic order is present for $D/J \geqslant 0.5$. Note that the tricritical point, represented by the letter **Q**, is at the vertical axis for $D/J = 0.462$. Its coordinates are $\mathbf{Q} = (0.00; 0.33)$. Thus, for $0.462 < D/J < 0.500$, the ferromagnetic region is enclosed only by a first-order line.

In this plane the topology of the phase diagram changes according to the value the D. The frontier separating the ferromagnetic and the paramagnetic phase contains a tricritical point for $0 < D/J \leqslant 0.462$, but for $0.462 < D/J < 0.500$ this frontier is only of first-order (see Fig. 12). It can also be observed the presence of the second ferromagnetic phase $\mathbf{F}'$ when $0.228 < D/J < 0.286$. The richest topology is found for $D/J = 0.25$, where four multicritical points appear [see Fig. 11(a)]. This topology is somewhat similar of that found in the phase diagram of two interacting spin-1/2 systems subject to a random field [51]. For $D < 0$, the phase diagram in the k_BT/J-K/J plane is qualitatively similar to the result of Kardar [6] ($D \to -\infty$).

Based on a previous study on the spin-1/2 case [6], we believe that the model analyzed in this paper will present a richer critical behavior when implemented in two- and three-dimensional lattices. This opens the possibility for further studies, where we can find experimental data to compare with the theoretical results. Furthermore, another relevant improvement study would be to control the competition through the value of an exponent α by considering each spin interaction in the first term of the Hamiltonian given in Eq. (2), as $J_{ij} = J/r_{ij}^{\alpha}$. So we could observe, through Monte Carlo simulations, how the topology of the phase diagrams changes with α.

ACKNOWLEDGMENT

This work was partially supported by CNPq and FAPEAM (Brazilian agencies).

APPENDIX: HUBBARD-STRATONOVICH TRANSFORMATION FOR THE ISING MODEL

In this Appendix we show briefly how the Hubbard-Stratonovich transformation and the saddle-point method work to get the free-energy density and the magnetization of the Ising model. The Hamiltonian of this model is as follows:

$$\mathcal{H} = -\frac{J}{2N}\left(\sum_{i=1}^{N} S_i\right)^2 - \sum_{i=1}^{N} \mathcal{H}_i'(S_i), \tag{A1}$$

where $S_i = -S \ldots S$ is a spin variable at site i, N is the number of spins, and $\mathcal{H}_i'(S_i)$ is some spin Hamiltonian containing short-range interactions in one dimension. For example, in this work we use

$$\mathcal{H}_i'(S_i) = K S_i S_{i+1} + \frac{D}{2}\left[S_i^2 + S_{i+1}^2\right] - \frac{H}{2}(S_i + S_{i+1}), \tag{A2}$$

where K is the nearest-neighbor interaction, D is the anisotropy parameter, and H the magnetic field. The canonical partition function for the general Hamiltonian is given by

$$Z = \sum_{\{S_i\}} e^{\frac{\beta J}{2N}(\sum_{i=1}^{N} S_i)^2} \prod_{i=1}^{N} e^{-\beta \mathcal{H}_i'}. \tag{A3}$$

In order to decouple the interaction between the spins $\{S_i\}$ in the first term of the exponential above, we use the Hubbard-Stratonovich transformation, which is expressed by

$$\exp\left\{\frac{ax^2}{2N}\right\} = \sqrt{\frac{Na}{2\pi}} \int_{-\infty}^{\infty} e^{-\frac{Nay^2}{2} + axy} dy. \tag{A4}$$

Accordingly, the partition function is now expressed by the following integral:

$$Z = \sqrt{\frac{N\beta J}{2\pi}} \int_{\infty}^{\infty} e^{-N\beta g(y)} dy, \tag{A5}$$

with

$$g(y) = \frac{J}{2} y^2 - \frac{1}{\beta N} \log[z(y)] \tag{A6}$$

and

$$z(y) = \sum_{\{S_i\}} \prod_{i=1}^{N} e^{\beta(JyS_i - \mathcal{H}_i')}. \tag{A7}$$

Note that the partial partition function (A7) can be obtained by using the matrix transfer method, where for the case of short-range Hamiltonian (2) with spin $S = 1 (S_i = -1,0,1)$ an analytic solution is found and for $S > 1$, it can only be found numerically.

The idea of the saddle-point method is to approximate the integral above by expanding the function $g(y)$ very close to its minimum y_0, because the negative exponential function is rapidly decreasing. So only the first three terms in the Taylor expansion of $g(y)$ are considered:

$$g(y) = g(y_0) + g'(y_0) + \tfrac{1}{2} g''(y_0)(y - y_0)^2 + \ldots. \tag{A8}$$

Before evaluating the integral, we may note that the first derivative is zero due to the fact that $g'(y_0)$ is null at its minimum. Also, after equating the explicit expression of $g'(y_0)$ to zero, we get an expression for the point y_0. Now the integral of the partition function is a Gaussian integral which can be easily evaluated:

$$\int_{-\infty}^{\infty} e^{-N\beta g(y)} dy \simeq e^{-N\beta g(y_0)} \int_{-\infty}^{\infty} e^{-\frac{N\beta}{2} g''(y_0)(y-y_0)^2} dy = \sqrt{\frac{2\pi}{N\beta g''(y_0)}} e^{-N\beta g(y_0)}, \tag{A9}$$

where $g''(y_0) > 0$, because y_0 is a minimum point. Thus, the partition function for a finite number of spins is approximately given by:

$$Z \simeq \sqrt{\frac{J}{\beta g''(y_0)}} e^{-N\beta g(y_0)}. \tag{A10}$$

In order to obtain the free-energy density we must take the following limit:

$$f = -\lim_{N\to\infty}\left\{\frac{\log Z}{N\beta}\right\} = \lim_{N\to\infty}\left\{g(y_0) - \frac{1}{2\beta N}\log\left[\frac{g''(y_0)}{J}\right]\right\} = g(y_0), \tag{A11}$$

where $g(y_0)$ corresponds to $f(y_0)$ in Eq. (6) in the thermodynamic limit ($N \to \infty$). Therefore, the free-energy density is a function of y_0,

$$f = g(y_0) = \frac{1}{2} J y_0^2 - \frac{1}{\beta} \log[z(y_0)]. \tag{A12}$$

Finally, we can show that y_0 is the magnetization per spin by taking the limit of the partial derivative of f with respect to the field H, when H tends to zero. Consequently, the magnetization per spin is the value of y at which the function $g(y)$ reaches its minimum.

In order to illustrate the above method, we use the Hamiltonian (2) for the spin $S = 1$ case; therefore, the partial partition function (A7) is written in the form

$$z(y) = \sum_{\{S_i\}} e^{\frac{\beta(H+Jy)}{2}(S_i + S_{i+1}) - \beta K S_i S_{i+1} - \frac{\beta D}{2}[S_i^2 + S_{i+1}^2]}. \tag{A13}$$

Using the transfer matrix technique, the Eq. (A13) can be rewritten as

$$z(y) = \sum_{S_i=-1}^{1} \langle S_i | W^N | S_i \rangle = \mathrm{Tr}\{W^N\} = \lambda_1^N + \lambda_2^N + \lambda_3^N, \tag{A14}$$

with

$$\mathbf{W} = \begin{bmatrix} e^{-\beta(H+Jy+K+D)} & e^{-\frac{\beta}{2}(H+Jy+D)} & e^{\beta(K-D)} \\ e^{-\frac{\beta}{2}(H+Jy+D)} & 1 & e^{\frac{\beta}{2}(H+Jy-D)} \\ e^{\beta(K-D)} & e^{\frac{\beta}{2}(H+Jy-D)} & e^{\beta(H+Jy-K-D)} \end{bmatrix}. \tag{A15}$$

where $\{\lambda_i, i = 1,2,3\}$ are the eigenvalues of the matrix $\mathbf{W}$ in Eq. (A15). Considering that $\lambda_1 = \lambda_{\max} > \lambda_2 > \lambda_3$ (maximum eigenvalue), and substituting Eq. (A14) in Eq. (A12), we obtain the following expression for the free-energy density:

$$f(y_0) = \frac{J y_0^2}{2} - \frac{1}{\beta} \log[\lambda_{\max}(y_0)], \tag{A16}$$

where

$$\lambda_{\max} = -\frac{A}{3} + 2\sqrt{Q}\cos\left(\frac{\theta}{3}\right), \tag{A17}$$

$$A = \mathrm{Tr}\{W\} = 1 + 2e^{-\beta(K+D)}\cosh[\beta(H+Jy)], \tag{A18}$$

$$B = 2e^{-\beta D}\cosh[\beta(H+Jy)] + e^{-\beta(D+H+Jy)} + 2e^{-2\beta D}\sinh(2\beta K) - 2e^{-\beta(K+D)}\cosh[\beta(H+Jy)], \tag{A19}$$

$$Q = \frac{A+3B}{9}, \tag{A20}$$

$$C = \det(W), \tag{A21}$$

$$R = \frac{9AB - 27C - 2A^3}{54}, \tag{A22}$$

$$\theta = \cos^{-1}\left[\frac{C}{Q^{3/2}}\right]. \tag{A23}$$

The magnetization $m = y_0$ is obtained by minimizing the free-energy density in Eq. (A16), i.e., $(\frac{\partial f}{\partial y})_{y=y_0}$, where the expression for m is given by

$$m = \frac{1}{\beta J}\left\{\frac{\partial \log[\lambda_{\max}(y)]}{\partial y}\right\}_{y=y_0=m} \equiv \psi(m). \tag{A24}$$

The results presented in this Appendix, can be applied for other values of the spin S, such that $S > 1$, including more interactions (next-nearest neighbors, etc.).

[1] Q. Si and F. Steglich, Science **329**, 1161 (2010).
[2] C. Lacroix, P. Mendels, and F. Mila, *Introduction to Frustrated Magnetism* (Springer-Verlag, Berlin, 2011).
[3] K. H. Fischer and J. A. Hertz, *Spin Glasses* (Cambridge University Press, Cambridge, 1991).
[4] M. J. Bueno, Jorge L. B. Faria, Alberto S. de Arruda, L. Craco, and J. R. de Sousa, J. Mag. Mag. Mat. **337**, 29 (2013).
[5] O. R. Salmon, J. Ricardo de Sousa, and F. D. Nobre, Phys. Lett. A **373**, 2525 (2009).
[6] M. Kardar, Phys. Rev. B **28**, 244 (1983).
[7] J. Jacob, A. Kumar, M. A. Anisimov, A. A. Povodyrev, and J. V. Sengers, Phys. Rev. E **58**, 2188 (1998).
[8] C. Tsallis, *Introduction to Nonextensive Statistical Mechanics: Approaching a Complex World* (Springer, New York, 2009).
[9] J. F. Nagle, Phys. Rev. A **2**, 2124 (1970).
[10] J. C. Bonner and J. F. Nagle, J. Appl. Phys. **42**, 1280 (1971).
[11] M. Kaufman and M. Kahana, Phys. Rev. B **37**, 7638 (1988).
[12] D. Mukamel, S. Ruffo, and N. Schreiber, Phys. Rev. Lett. **95**, 240604 (2005).
[13] O. Cohen, V. Rittenberg, and T. Sadhu, J. Phys. A: Math. Theor. **48**, 055002 (2015).
[14] G. A. Baker, Jr., Phys. Rev. **130**, 1406 (1963).
[15] M. Kaufman and M. Kardar, Phys. Rev. B **30**, 1609(R) (1984).
[16] M. Kardar and M. Kaufman, Phys. Rev. Lett. **51**, 1210 (1983).
[17] A. Campa, T. Dauxois, and S. Ruffo, Phys. Rep. **480**, 57 (2009).
[18] M. Blume, Phys. Rev. **141**, 517 (1966).
[19] H. W. Capel, Physica **32**, 966 (1966).
[20] M. Blume, V. J. Emery, and R. B. Griffiths, Phys. Rev. A **4**, 1071 (1971).
[21] B. L. Arora and D. P. Landau, in *Magnetism and Magnetic Materials*, edited by C. D. Graham, Jr. and J. J. Rhyne, AIP Conf. Proc. No. 5 (AIP, New York, 1972), p. 352.
[22] A. F. Siqueira and I. P. Fitipaldi, Phys. Stat. Sol. (b) **119**, K31 (1983).
[23] P. D. Beale, Phys. Rev. B **33**, 1717 (1986).
[24] T. Kaneyoshi, J. Phys. C: Solid State Phys. **19**, L557 (1986).
[25] T. Kaneyoshi, Physica A **182**, 436 (1992).
[26] C. M. Care, J. Phys. A **26**, 1481 (1993).
[27] C. J. Silva, A. A. Caparica, and J. A. Plascak, Phys. Rev. E **73**, 036702 (2006).
[28] M. Clusel, J.-Y. Fortin, and V. N. Plechko, J. Phys. A: Math. Theor. **41**, 405004 (2008).
[29] X. Y. Chen, Q. Jiang, W. Z. Shen, and C. G. Zhang, J. Mag. Mag. Mat. **262**, 258 (2003).
[30] F. Litaiff, J. Ricardo de Sousa, and N. S. Branco, Solid State Commun. **147**, 494 (2008).
[31] T. Dauxois, P. de Buy, L. Lori, and S. Ruffo, J. Stat. Mach. (2010) P06015.
[32] Edited by T. Dauxois, S. Ruffo, E. Arimondo, and M. Wilkens, *Dynamics and Thermodynamics of Systems with Long-Range Interactions*, Lecture Notes in Physics, Vol. 602 (Springer, Berlin, 2002).
[33] Edited by A. Campa, A. Giansanti, G. Morigi, and F. Sylos Labini, *Dynamics and Thermodynamics of Systems with Long-Range Interactions: Theory and Experiments*, AIP Conf. Proc. No. 970 (AIP, New York, 2008).
[34] Edited by T. Dauxois, S. Ruffo, and L. Cugliandolo, *Long-Range Interactions: Les Houches Summer School* (Oxford University Press, Oxford, 2009).
[35] A. S. Chernyi, E. N. Khatsko, A. I. Rykova, and A. V. Eremenko, Low Temp. Phys. **38**, 843 (2012).
[36] L. J. de Jongh, W. D. Van Amstel, and A. R. Miedema, Physica **58**, 277 (1972).
[37] L. J. de Jongh, A. C. Botterman, F. R. de Boer, and A. R. Miedema, J. Appl. Phys. **40**, 1363 (1969).
[38] P. Bloembergen, K. G. Tan, F. H. J. Lefevre, and A. H. M. Bleyendaal, J. Phys. Colloques **32**, C1-878 (1971).
[39] L. J. de Jongh and W. D. van Amstel, J. Phys. Colloques, **32**, C1-880 (1971).
[40] A. R. Miedema, J. Phys. Colloques, **32**, C1-305 (1971).
[41] M. Sato and A. J. Sievers, Nature **432**, 486 (2004).
[42] M. Sato and A. J. Sievers, Phys. Rev. B **71**, 214306 (2005).

[43] J. P. Wrubel, M. Sato, and A. J. Sievers, Phys. Rev. Lett. **95**, 264101 (2005).
[44] G. Chapuis, G. Brunisholz, C. Javet, and R. Roulet, Inorg. Chem. **22**, 455 (1983).
[45] K. Huang, *Statistical Mechanics*, 2nd ed. (John Wiley & Sons, New York, 1987).
[46] V. Dotsenko, *Introduction to the Replica Theory of Disordered Statistical Systems* (Cambridge University Press, Cambridge, 2001).
[47] H. Nishimori, *Statistical Physics of Spin Glasses and Information Processing* (Oxford University Press, Oxford, 2001).
[48] M. Kaufman, Phys. Rev. B **39**, 6898 (1989).
[49] R. B. Griffiths, Phys. Rev. B **12**, 345 (1975).
[50] Octavio D. R. Salmon and J. Rojas, J. Phys. A: Math. Theor. **43**, 125003 (2010).
[51] Octavio D. Rodriguez Salmon and F. D. Nobre, Phys. Rev. E **89**, 062104 (2014).